


Quantum optimal control without arbitrary waveform generators

Qi-Ming Chen^{1,2,3}, Herschel Rabitz^{2,*} and Re-Bing Wu^{3,†}

¹*QCD Labs, QTF Centre of Excellence, Department of Applied Physics, Aalto University, Aalto FI-00076, Finland*

²*Department of Chemistry, Princeton University, New Jersey 08544, USA*

³*Department of Automation, Tsinghua University, Beijing 100084, China*

 (Received 20 September 2022; revised 1 August 2023; accepted 16 November 2023; published 8 December 2023)

Simple, precise, and robust control is demanded for qubit operations on large quantum information processors. However, existing routes to high-fidelity quantum control heavily rely on arbitrary waveform generators that are difficult to scale up. Here, we show that the arbitrary control of a quantum system can be achieved by simply turning the control fields on and off in a proper sequence. The switching instances can be designed using conventional quantum optimal control algorithms, while the required computational resources for matrix exponentials can be substantially reduced. We demonstrate the flexibility and robustness of the resulting control protocol, and illustrate it in the context of superconducting quantum circuits. We expect this proposal to be achievable with current semiconductor and superconductor technologies, which offers a significant step towards scalable quantum computing.

DOI: [10.1103/PhysRevApplied.20.064016](https://doi.org/10.1103/PhysRevApplied.20.064016)

I. INTRODUCTION

The desire to control quantum-mechanical phenomena has been growing rapidly with the development of quantum information processors [1,2]. Moving beyond the attempts at seeking physically intuitive control fields, quantum optimal control (QOC) opens the prospect of reaching high-fidelity quantum operations with modulated waveforms [3–6]. For many years, QOC has been successfully applied to various physical platforms, such as superconducting quantum circuits (SQCs) [7–27]. Arbitrary waveform generators (AWGs) have become indispensable for high-fidelity quantum control. However, towards the control of quantum information processors with hundreds of qubits, the brute-force scaling of current AWG technologies involves substantial overhead in experimental resources. Additionally, integrating arrays of AWGs at low temperature remains a technical challenge [28–35]. Besides these efforts of pursuing the ability of generating more delicate waveforms, a natural question is whether QOC necessarily requires a fully arbitrary waveform.

Here, we report that the generation of arbitrary control waveforms can be equivalently realized by simply turning on and off the driving fields at prescribed time instances [36]. This method is motivated by the pulse width modulation (PWM) technique in power electronic devices, where the average power delivered to the plant is controlled by switching the supply at a fast rate and

particular pattern [37]. We generalize this idea to quantum-mechanical systems and reveal the equivalence between an arbitrary waveform and a PWM pulse train. We also show that a PWM sequence can be efficiently designed with existing QOC algorithms, and demonstrate its robustness and flexibility in possible experimental implementation. These results indicate a simple, precise, robust, and scalable quantum control protocol that may greatly facilitate the building of large controlled quantum systems.

II. THE PWM CONTROLLER

A. Waveform-pulse train correspondence

We consider a general system with the drift (time-independent) Hamiltonian H_0 and the control (time-dependent) Hamiltonian $H_c(t) = \sum_{k=1}^K u_k(t)H_k$, where H_k is Hermitian and $u_k(t)$ is a real function of time serving as the k th control field. Assuming that there exists an optimal waveform $u_k(t)$ that maximizes a chosen objective $J(T)$ at the final time T , the key foundation of the PWM method is that there always exists a pulse train $s_k(t)$ that achieves the same goal to an arbitrary precision (see Appendix A).

To be specific, we formally define a PWM sequence as

$$s_k(t) = \sum_{m=1}^M \xi_k [\theta(t - \tau_{k,m}^{\text{on}}) - \theta(t - \tau_{k,m}^{\text{off}})], \quad (1)$$

where $\theta(t)$ is the Heaviside step function, $M = T/\tau$ is the number of pulses in the time interval $[0, T]$. Physically, the pulse train may be generated by operating an ideal switch

*hrabitz@princeton.edu

†rbwu@tsinghua.edu.cn

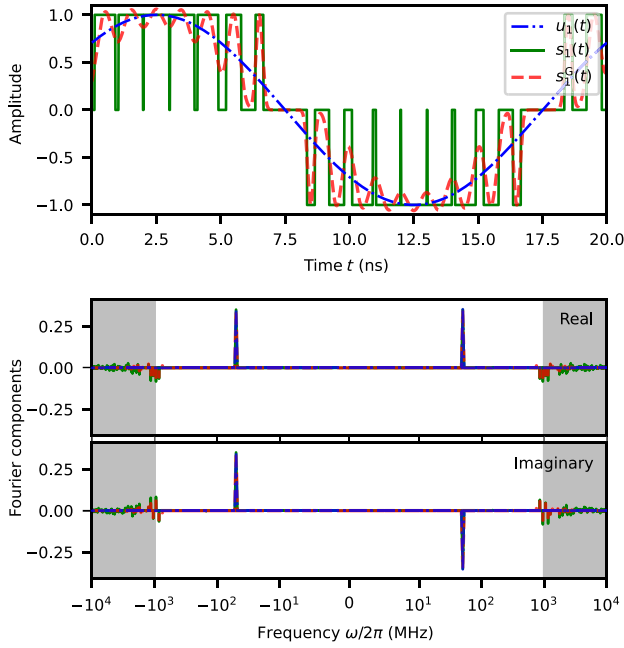


FIG. 1. Comparison between a sinusoidal waveform, $u_1(t) = \sin(\omega t + \pi/4)$ for $\omega/2\pi = 50$ MHz (blue, dash-dot), and a sequence of rectangular or Gaussian pulses, $s_1(t)$ (green, solid) and $s_1^G(t)$ (red, dashed), respectively, in both the time domain and frequency domain. Here, we have used $M = 20$ pulses to approximate the waveform in each period. The three functions show almost the same Fourier components below a prescribed threshold $\Omega_1/2\pi \approx 1$ GHz. The difference manifests mainly in the high-frequency regime (shaded area).

at time instances $\tau_{k,m}^{\text{on/off}} = m\tau - (\tau \pm |\tau_{k,m}|)/2$, where

$$\tau_{k,m} = \int_{(m-1)\tau}^{m\tau} u_k(t) dt / \xi_k. \quad (2)$$

Here, $|\tau_{k,m}|$ represents the pulse width in the m th interval, and $\text{sgn}[\tau_{k,m}]\xi_k$ with $\xi_k = \max |u_k(t)|$ is the amplitude of the pulse train, as illustrated in Fig. 1. For any specific waveform $u_k(t)$, the only free parameter of the PWM sequence is the number of pulses M in the time interval T , while $\tau_{k,m}$ is automatically determined by the integral of $u_k(t)$ in each time interval T/M . Parameter ξ_k can be selected in different ways, which will be discussed in Sec. II C.

Although the two fields $u_k(t)$ and $s_k(t)$ are vastly different in the time domain, their Fourier components are almost identical below a prescribed threshold, $\Omega_k/2\pi \approx 1/\tau$, in frequency. The higher-frequency components above $\Omega_k/2\pi$ are relatively small compared with the major frequency components within $\pm\Omega_k/2\pi$. They can be ignored if the characteristic frequency of the system is much smaller than $\Omega_k/2\pi$, or may be physically filtered out in experiments. A numerical study with additional filters will be provided in Sec. IV A. Given a prescribed

cutoff frequency $\Omega_f/2\pi$, one may always choose $\tau \ll 2\pi/\Omega_f$ such that an arbitrary waveform $u_k(t)$ and a pulse train with the same amplitude, $s_k(t)$, have the identical spectrum within the desired bandwidth.

In the time domain, we use the Dyson series to calculate the average short-time propagation operator for each time interval $U[m\tau, (m-1)\tau]$ and compare it with the ideal propagator generated by $u_k(t)$. One can prove that the PWM sequence results in a second-order approximation to the ideal unitary propagation, i.e., $\delta U[m\tau, (m-1)\tau] \propto \mathcal{O}(\tau^3)$, which is independent of the number of control degrees of freedom K (see Appendix B). This accuracy is at the same order of the staircase approximation of a waveform generated by AWGs, which supports the equivalence between a continuous and a pulsed control protocol.

B. Imperfect switches

We now study the robustness of the PWM protocol with respect to two imperfect switching events: (i) time jitter and (ii) finite switching speed. For (i), we assume that the m th pulse width deviates from the design value by $\delta\tau_{k,m}$, which obeys a Gaussian distribution with mean value *zero* and standard deviation σ_k [38]. Then, $\delta\tau_{k,m}\delta\tau_{k',m}/\sigma_k\sigma_{k'}$ obeys the χ^2 distribution with expectation value 1 for $k = k'$, or the generalized Laplace distribution with expectation value *zero* elsewhere. Taking the average of the Dyson-series form of the short-time propagator and keeping only the leading-order terms of σ_k , we find that the expectation value of the deviation is $\langle \delta U[m\tau, (m-1)\tau] \rangle \approx \sum_{k=1}^K \sigma_k^2 \xi_k^2 H_k^2 / 2$, where $\langle \cdot \rangle$ is the ensemble average. The second-order dependance of σ_k leads to favorable error scaling, i.e., the time jitter with $\sigma_k = \tau_{k,m}/100$ causes only a 0.01% relative error that may be neglected for $T \simeq 10^3 \tau$ [39].

To account for the influence of a finite switching speed, (ii), we consider a sequence of Gaussian pulses

$$s_k^G(t) = \sum_{m=1}^M \xi_k e^{-\pi[t - (m-1/2)\tau]^2 / \tau_{k,m}^2}, \quad (3)$$

where $\tau_{k,m}$ is defined in Eq. (2). The bell-like edges and the overlap between adjacent pulses describe a relatively slow switch, which distorts the desired rectangular pulses. Nevertheless, one can prove that the Fourier components of $s_k^G(t)$ are identical to the ideal case below Ω_k (see Appendix D), as illustrated in Fig. 1. Thus, the control performance has the same order of precision as the perfect rectangular pulses.

C. Generalizations

The waveform-pulse train correspondence can be generalized to design PWM control protocols in a variety of ways, for example, by removing the $s_k(t) = 0$ stage of the

sequence. The resulting binary sequence is called the 2-level PWM pulse sequence in the literature, which keeps the signal power unchanged and alters only the polarization of the switch. Similarly, one can also define an n -level PWM sequence with n discrete polarizations of $s_k(t)$. From another perspective, one may stretch the pulse magnitude ξ_k by a factor of κ and shrink the pulse width by $1/\kappa$ at the same time, while keeping the spectrum, and therefore the control performance, almost unchanged. The extreme case with $\kappa \rightarrow \infty$ represents a sequence of hard control pulses that apply instantaneous but non-negligible kicks to the system [40–42]. Here, the corresponding time propagation is identical to the symmetrically decomposed Suzuki-Trotter formula [43,44]

$$U[m\tau, (m-1)\tau] = \left(\prod_{k=0}^K e^{-i\tau_{k,m}\xi_k H_k/2} \right) \left(\prod_{k=K}^0 e^{-i\tau_{k,m}\xi_k H_k/2} \right), \quad (4)$$

where $\tau_{0,m} = \tau$ and $\tau_{k,m}$ is the pulse width defined in Eq. (2). Detailed analysis shows that Eq. (4) has a slightly larger error rate than the $\kappa = 1$ case, as the high-frequency components above Ω_k are stronger (see Appendix D). However, the instant-time system Hamiltonian $H(t)$ takes values from a smaller discrete set, $H(t) \in \{H_0, \pm\xi_1 H_1, \dots, \pm\xi_K H_K\}$. This simplification makes the simulation of the time-dependent Schrödinger equation (TDSE) even more efficient without substantially deteriorating the numerical precision.

Using the high-order form of the Suzuki-Trotter formula [45–47], one can insert more pulses in each time interval and increase the precision for solving TDSE and also for physical implementations. One can prove that the $(2n+1)$ th-order-accurate PWM sequence, with all the pulse widths being real and positive, always exists. The corresponding number of pulses in each interval is 3^{2n-1} , where the new pulse widths can be derived from the second-order-accurate form (see Appendix D). By comparison, the accuracy of the staircase approximation remains at the second order when splitting each short time interval by the same number of pieces.

III. DESIGN OF THE PWM SEQUENCE

In the material above, we have discussed how to approximate a well-designed optimal control field $u_k(t)$ by a PWM sequence $s_k(t)$. We can also design an optimal-control PWM sequence directly from the numerical algorithms. Similar to Eq. (1), we describe an arbitrary but digitally sampled time-dependent signal by a summation

of rectangular pulses

$$y_k(t) = \sum_{m=1}^M \xi_{k,m} \left\{ \theta \left[t - \left(t_{k,m} - \frac{|\tau_{k,m}|}{2} \right) \right] - \theta \left[t - \left(t_{k,m} + \frac{|\tau_{k,m}|}{2} \right) \right] \right\}. \quad (5)$$

This definition describes a sequence of rectangular pulses that are centered at time $t_{k,m}$ for $m = 1, \dots, M$ with width $\tau_{k,m}$ and height $\xi_{k,m}$.

When fixing the values of $t_{k,m} = (m+1/2)T/M$ and $\tau_{k,m} = T/M$ and varying $\xi_{k,m}$ for different m , $y_k(t)$ describes a staircase waveform generated by an AWG. Alternatively, we can fix the values of $\tau_{k,m}$ and $\xi_{k,m}$ but vary $t_{k,m}$ for different m . In this case, $y_k(t)$ consists of a sequence of identical pulses with controllable pulse centers in the time domain. The resulting control field is denoted as a pulse frequency modulation (PFM) sequence in classical control systems. A typical example of PFM is the rapid single flux quantum (RSFQ) sequence in the context of SQC if, for each individual pulse, the time integral over voltage is identical to a single flux quantum [48–52]. One missing combination among the three procedures is the PWM sequence proposed in this study. Here, we fix the values of $t_{k,m} = (m+1/2)T/M$ and $\xi_{k,m}$ but vary $\tau_{k,m}$ for different m . This describes a sequence of evenly spaced pulses in time but with adjustable widths.

Besides the above three combined methods, one may design more general control fields with two constraints on the three parameters. The number of free parameters thus remains as $K \times M$. One prominent example is the method of bang-bang control, which is composed of a fixed parameter $\xi_{k,m}$ and the linear constraint $(\tau_{k,m} + \tau_{k,m+1})/2 = (t_{k,m+1} - t_{k,m})$. The function $y_k(t)$ thus switches between $\pm\xi_k$ in time [53–56]. Following this procedure, one may come up with many other combinations among the three parameters $\xi_{k,m}$, $t_{k,m}$, and $\tau_{k,m}$ that may be suitable for specific implementations.

A. Pulse train optimization

With these understandings in mind, the optimization of a PWM sequence is as straightforward as that for AWG [3] and PFM or RSFQ [49]. One may simply treat the pulse widths $\tau_{k,m}$ as control variables and resort to numerical algorithms. The optimization problem can be written in the standard form as

$$\max_{\{\tau_{k,m}\}} J(T, \{\tau_{k,m}\}), \quad (6)$$

which is subject to the Schrödinger equation. The optimization is under the constraint that $|\tau_{k,m}| \leq \tau$, so as to avoid overlap between two adjacent pulses in the sequence.

When the pulse number M is not large, it is convenient to apply gradient-free iterative algorithms to optimize $\tau_{k,m}$ for $m = 1, \dots, M$. However, gradient-decent algorithms are preferable for large M because of their shorter convergence time. The exact gradient formula for a PWM sequence is rather complex when considering multiple control fields. Here, we provide two approximate gradient formulas.

The first formula is based on the standard gradient formula for the AWG-based control fields

$$\frac{\partial U(T, 0)}{\partial u_{k,m}} = -i\tau U[T, (m+1)\tau] H_k U[m\tau, 0]. \quad (7)$$

The second gradient formula comes from the Suzuki-Trotter form of the pulsed propagation operator, i.e., Eq. (4) in Sec. II C. We have

$$\begin{aligned} \frac{\partial U(T, 0)}{\partial s_{k,m}} = & -\frac{i\xi_k}{2} U[T, (m+1)\tau] \left[\left(\prod_{k=0}^m e^{-i\tau_{k,m} H_k/2} \right) H_k \left(\prod_{k=m+1}^K e^{-i\tau_{k,m} H_k/2} \right) \left(\prod_{k=K}^0 e^{-i\tau_{k,m} H_k/2} \right) \right. \\ & \left. + \left(\prod_{k=0}^K e^{-i\tau_{k,m} H_k/2} \right) \left(\prod_{k=m}^0 e^{-i\tau_{k,m} H_k/2} \right) H_k \left(\prod_{k=K}^{m+1} e^{-i\tau_{k,m} H_k/2} \right) \right] U[(m-1)\tau, 0]. \end{aligned} \quad (10)$$

One can cross-check the consistency of the two gradient formulas by rearranging H_k in Eq. (10) to the front of the brackets and using Eq. (4) to simplify the notation. The result is identical to Eq. (9). This is essentially the same as approximating a time-ordered integral by a normal integral when τ is sufficiently small.

B. Numerical acceleration

A good QOC algorithm needs both quick convergence and efficient calculation of the propagation operator $U(T, 0)$ for solving the TDSE. The latter requires a considerable number of numerically expensive matrix exponentials in each iteration of the optimization [57]. The PWM approach circumvents this technical challenge by exact

The waveform-pulse train correspondence implies the following expression for a PWM sequence:

$$s_{k,m} = u_{k,m} \tau / \xi_k. \quad (8)$$

Combining the two equations above and applying the chain rule, we obtain the first gradient formula

$$\frac{\partial U(T, 0)}{\partial s_{k,m}} = -i\xi_k U[T, (m+1)\tau] H_k U[m\tau, 0]. \quad (9)$$

Depending on the specific definition of the fidelity function $J(T)$, the gradient of fidelity with respect to $s_{k,m}$ can be obtained straightforwardly.

matrix decomposition, and may significantly accelerate the calculation. Because $s_k(t)$ can be either *zero* or $\pm\xi_k$, the system Hamiltonian at any time instance is chosen from a finite set

$$\begin{aligned} H(t) \in \{ & H_0, H_0 + \xi_1 H_1, H_0 - \xi_1 H_1, H_0 + \xi_2 H_2, \dots, \\ & H_0 + \dots + \xi_K H_K, \dots, H_0 - \dots - \xi_K H_K \}. \end{aligned} \quad (11)$$

Thus, one may diagonalize these Hamiltonians in advance and convert the matrix exponentials into scalar exponentials and matrix products. As a concrete example, we consider the simplest case with one unique control field, $K = 1$. The propagator for the m th time interval can be written as

$$U[m\tau, (m-1)\tau] = \begin{cases} P_0 \exp \left[-i \left(\tau + \frac{\tau_{1,m}}{2} \right) \Lambda_0 \right] P_0^\dagger P_- \exp [+i\tau_{1,m} \Lambda_-] P_-^\dagger P_0 \exp \left[-i \left(\tau + \frac{\tau_{1,m}}{2} \right) \Lambda_0 \right] P_0^\dagger & \text{for } \tau_{1,m} < 0, \\ P_0 \exp \left[-i \left(\tau - \frac{\tau_{1,m}}{2} \right) \Lambda_0 \right] P_0^\dagger P_+ \exp [-i\tau_{1,m} \Lambda_+] P_+^\dagger P_0 \exp \left[-i \left(\tau - \frac{\tau_{1,m}}{2} \right) \Lambda_0 \right] P_0^\dagger & \text{for } \tau_{1,m} \geq 0, \end{cases} \quad (12)$$

with $H_0 = P_0 \Lambda_0 P_0^\dagger$, $H_0 \pm \xi_1 H_1 = P_\pm \Lambda_\pm P_\pm^\dagger$. Here, Λ_0 (Λ_\pm) and P_0 (P_\pm) are real diagonal and unitary matrices, respectively, and the \pm sign indicates the

polarization of the pulse in the m th time interval. This diagonalization process describes the change of basis for representing the matrices H_0 and $H_0 \pm \xi_1 H_1$ such that they

are always written in a diagonal form. In each of the bases, the time propagation induces only a phase factor in the corresponding eigenstates, while the change between the bases captures the possible state transition processes and can be efficiently calculated.

This trick is similar to the split operator method for solving TDSE [58–60]. Assuming that the Hilbert space is d dimensional, the propagation operator requires the calculation of $(K + 1)$ diagonal matrix exponentials and $(K + 1)$ products between a diagonal matrix and a general matrix. The floating-point operations (FLOPs) for both of the two types of operations are at the d^2 level. In comparison, the most time-consuming part is the product between two arbitrary matrices. The expression given in Eq. (12) requires $2(K + 1)d^3$ FLOPs in general with the P matrices and their combinations known in advance. However, one may save d^3 FLOPs when considering long-time propagation, since P_0 and P_0^\dagger always exist as the first and last terms of each short-time propagator and can cancel with each other. In total, the above calculation requires approximately $2Kd^3$ FLOPs once the decomposition is obtained.

By comparison, the typical method of matrix exponentiation, i.e., the scaling and squaring method based on the Padé approximation, generally requires $10d^3$ to $20d^3$ FLOPs depending on the specific problem and the detailed implementation [57]. Thus, the pulsed time propagation can be efficiently calculated for a relatively small number of control degrees of freedom, i.e., $K \lesssim 5\text{--}10$. As we show in Sec. IV B below, the above estimation of FLOPs is qualitatively consistent with the simulation results. We emphasize that the PWM approach requires $\mathcal{O}(d^2)$ FLOPs for state propagation problems where the initial state is fixed, which is one order of magnitude faster than the typical Padé approximation method [57].

C. Applicability considerations

The key foundation of the PWM method is the waveform-pulse train correspondence, which holds below the frequency threshold $\omega \leq \Omega_k$ with $\Omega_k/2\pi \approx 1/\tau$. It therefore limits the applicability of the PWM method to practical quantum control systems where τ is lower bounded by the realistic devices. For a qualitative estimation of the applicability, we define δ_s as the switching speed. The shortest single pulse it may achieve should have a duration of around $\tau_{k,m} \simeq 2\delta_s$. This equation indicates the upper bound on the threshold frequency, $\Omega_k/2\pi \simeq 1/(2\delta_s)$, which is the highest control bandwidth one may achieve. Considering that $\tau_{k,m}$ is not constant for different m in a general PWM sequence, and also that the waveform-pulse train correspondence is second-order accurate by default, we may relax the useful control bandwidth to $\Omega_k/2\pi \simeq 1/(50\delta_s)$.

To date, most of the available electronic devices are based on the complementary metal-oxide-semiconductor

(CMOS) technology, which has a typical switching speed of around $\delta_s \simeq 100$ ps. This technical limitation indicates that the best achievable control bandwidth is around 200 MHz for a PWM sequence. We note that there are already high-sampling rate CMOS controllers available, such as Keysight M8195A [61], which may push this limit to about 2 GHz. On the other hand, the RSFQ technology may significantly improve the control bandwidth to about the 20 GHz level. A drawback is the requirement of operation at cryogenic temperature. The RSFQ-based pulse generator is also not commercially available [62–65].

A potential means to circumvent the bandwidth limitation is to mix the control signal with a fast carrier wave, which is a standard technique in many experimental platforms, such as SQC. Here, the controller generates a slow-varying envelope, which is used to modulate the carrier wave that is approximately resonant to the relevant transition frequency. This technique is applicable when all the relevant transition frequencies lie in a small frequency range around the carrier-wave frequency. For SQC, this range is typically at about the 500-MHz scale. It is therefore possible to use the currently available high-sampling rate AWGs to generate the PWM sequence for QOC tasks.

IV. APPLICATION TO SQC

For illustration, we consider a chain of superconducting artificial atoms with XY control, $u_{n,x/y}(t)$ for $n = 1, \dots, N$. Here, each artificial atom is modeled as a Kerr-nonlinear resonator with annihilation and creation operators a_n and a_n^\dagger , of which the lowest two energy levels, $|0_n\rangle$ and $|1_n\rangle$, are encoded as a qubit. In the doubly rotating frame at the qubit frequency, the total Hamiltonian reads [18–22]

$$H = \sum_{n=1}^N \frac{\eta_n}{2} a_n^\dagger a_n^\dagger a_n a_n + \sum_{n=1}^{N-1} g_{n,n+1} (a_n^\dagger a_{n+1} + a_n a_{n+1}^\dagger) + \sum_{n=1}^N [u_{n,x}(t)(a_n + a_n^\dagger) + iu_{n,y}(t)(a_n - a_n^\dagger)]. \quad (13)$$

For simplicity, we truncate the Hilbert space of each artificial atom to three dimensions, and assume that all the atoms are homogeneous with anharmonicity $\eta_n/2\pi = -200$ MHz and coupling strength $g_{n,n+1}/2\pi = 30$ MHz. We evaluate the control performance by the average fidelity over all the relevant qubit states [66,67]

$$J(T) = \frac{\text{tr}[U(T, 0)PU^\dagger(T, 0)P] + |\text{tr}[U_g^\dagger U(T, 0)P]|^2}{2^N(2^N + 1)}, \quad (14)$$

where $P = \bigotimes_{n=1}^N (\mathbb{1}_n - |2_n\rangle\langle 2_n|)$ is the projection operator onto the qubit subspace and U_g is the target gate. In the following simulations, we use the Nelder-Mead algorithm

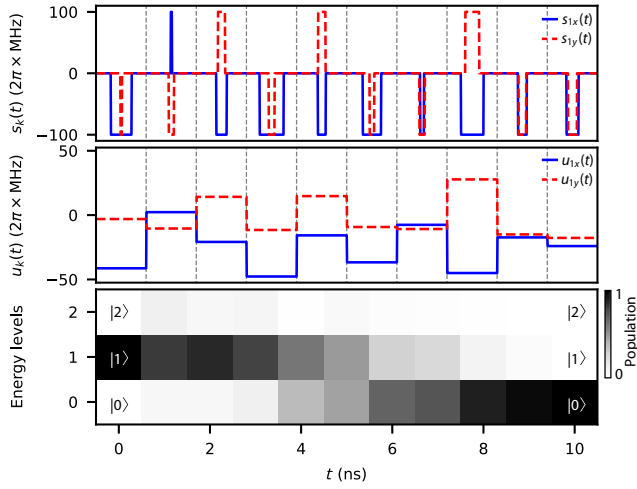


FIG. 2. The optimized single-qubit control pulse train (top) and the corresponding staircase waveform (middle). The bottom panel shows the dynamics of the system during the control process, where the population of $|1\rangle$ is transferred to $|0\rangle$ with 0.9999 fidelity.

to find the optimal control PWM sequences [68]. We are particularly interested in the following gates: the single-qubit NOT gate ($\text{NOT} = \sigma_{1,x}$), the two-qubit controlled-NOT (CNOT) gate ($\text{CNOT} = |1_1\rangle\langle 1_1|\sigma_{2,x} + |0_1\rangle\langle 0_1|\mathbb{1}_2$), the three-qubit controlled-controlled-Z (CCZ) gate [$\text{CCZ} = -|1_1 1_2\rangle\langle 1_1 1_2|1_3 + (|0_1 0_2\rangle\langle 0_1 0_2| + |0_1 1_2\rangle\langle 0_1 1_2| + |1_1 0_2\rangle\langle 1_1 0_2|)\mathbb{1}_3$], and the controlled-CNOT (CCNOT; Toffoli) gate [$\text{CCNOT} = |1_1 1_2\rangle\langle 1_1 1_2|\sigma_{3,x} + (|0_1 0_2\rangle\langle 0_1 0_2| + |0_1 1_2\rangle\langle 0_1 1_2| + |1_1 0_2\rangle\langle 1_1 0_2|)\mathbb{1}_3$]. Here, $\sigma_{n,i}$ denotes the standard Pauli- $(i = x, y, z)$ matrices in the n th-qubit subspace.

A. Single-qubit gate

We first study the $N = 1$ case with $T = 10$ ns and $\xi_{1,x/y}/2\pi = 100$ MHz. Our goal is to implement a NOT gate while preventing population leakage from the qubit subspace to higher-energy levels [7–12]. The optimized pulse trains and the converted staircase waveforms are respectively shown in the top and middle panels of Fig. 2, of which the fidelities are 0.9999 and 0.9997 [69]. Here, the conversion is achieved by inverting Eq. (2), i.e., $u_k(m\tau) = \xi_k \tau_{k,m}/\tau$, with $\tau = 1$ ns time resolution for the waveform. This result clearly indicates the correspondence between an arbitrary waveform and a pulse train, which is the basis of the PWM method. Furthermore, it demonstrates that a sequence of properly concatenated pulses can eliminate leakage in controlling a superconducting qubit, although each single pulse is broad in frequency and covers multiple energy levels. The detailed transfer among the three energy levels during the control process is illustrated in the bottom panel of Fig. 2, where the system is initially in $|1_1\rangle$.

To confirm the capability of leakage suppression, we test the performance of the optimized PWM sequence with different energy-level truncations, as shown in Fig. 3. Here,

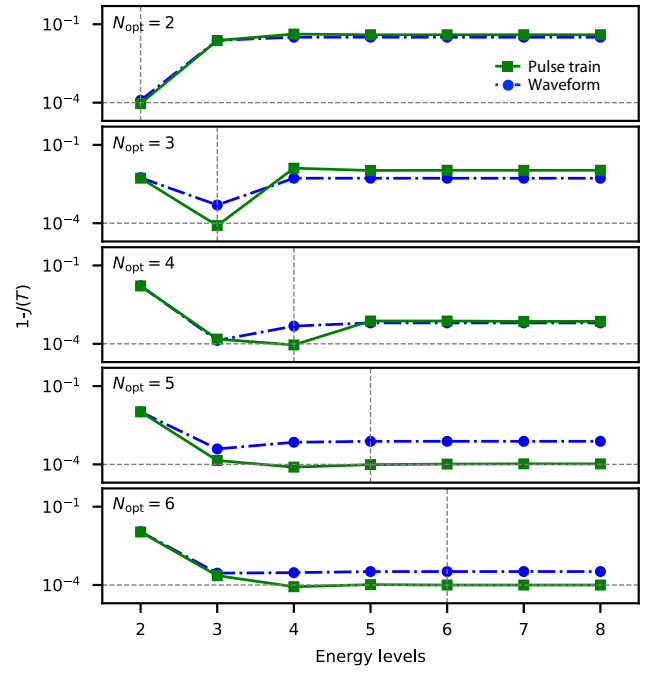


FIG. 3. Gate fidelity $J(T)$ with optimized control pulses versus the number of energy levels in the simulation. Here, N_{opt} is the number of energy levels chosen for optimization. The population leakage to higher-energy levels is avoided for $N_{\text{opt}} \geq 5$.

we denote by N_{opt} the chosen number of energy levels when utilizing the optimization algorithm. Because of the small anharmonicity α , higher-energy levels are inevitably populated when applying the control fields. The amount of leakage is almost the same for waveform and pulse sequence controls in all of our simulations. A straightforward solution to prevent the leakage is to choose a larger N_{opt} when performing the optimization. This is feasible because the transition frequency between any two adjacent energy levels becomes increasingly large for higher-energy levels of a Kerr resonator. For example, the $|1\rangle \leftrightarrow |2\rangle$ transition is detuned from the qubit transition frequency ($|0\rangle \leftrightarrow |1\rangle$) by α , while it is 2α for $|2\rangle \leftrightarrow |3\rangle$ and 3α for $|3\rangle \leftrightarrow |4\rangle$. We observe that $N_{\text{opt}} = 5$ is sufficient to avoid any possible population leakage when applying a PWM sequence.

We further consider a finite frequency cutoff, $\Omega_f/2\pi$, to the optimized PWM sequence, which describes the finite bandwidth of an actual device. The finite bandwidth rounds off the sharp corners of the rectangular pulses, as shown in Fig. 4. With the decrease of $\Omega_f/2\pi$ from 2 GHz to 250 MHz, the filtered PWM sequence tends to be constant in the time domain, while the corresponding gate fidelity decreases only from $J(T) = 0.9998$ to 0.9585. This is consistent with the expectation that the major control task of the NOT gate is implemented by the dc part of the control field, which is to be modulated with the carrier wave resonating at the qubit transition frequency.

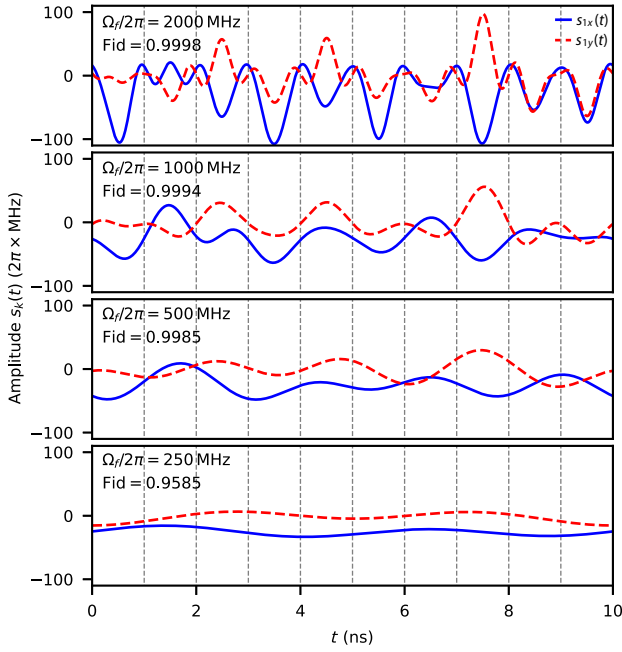


FIG. 4. The optimized single-qubit control pulse train under different cutoff frequencies $\Omega_f/2\pi$. The corresponding gate fidelity decreases from 0.9998 to 0.9585 when $\Omega_f/2\pi$ decreases from 2 GHz to 250 MHz. Here, the unfiltered sequence is the same as that in Fig. 2.

B. Multiqubit gate and numerical efficiency

Next, we consider the implementation of a CNOT gate with $N = 2$ and $\xi_{n,x/y}/2\pi = 100$ MHz. The fidelity is optimized to 0.9999 using pulse trains, while that of the converted waveforms is 0.9848. Similarly, we illustrate the dynamics of the system in Fig. 5(a), where the initial state $|1_10_2\rangle$ is transferred to $|1_11_2\rangle$ at $T = 20$ ns. We also optimized the pulse trains for implementing a 0.9999-fidelity CCZ gate at $T = 30$ ns with three ± 700 -MHz-range Z controls. The fidelity of the converted waveform is 0.9195. Qualitatively, the implementation of the CCZ gate is equivalent to the CCNOT (Toffoli) gate since $\text{CCNOT} = [\mathbb{1} \otimes \mathbb{1} \otimes \text{H}]\text{CCZ}[\mathbb{1} \otimes \mathbb{1} \otimes \text{H}]$, where H is the single-qubit Hadamard gate [13]. We therefore illustrate the dynamics of the system with two perfect Hadamard gates applied at the initial and final time, as shown in Fig. 5(b). These examples demonstrate the potential of using a PWM control protocol for realizing the universal control of superconducting qubits.

For more complex systems, we compare the computational efficiency of the PWM and the conventional approaches for solving TDSE (see Appendix C), as shown in Fig. 5(c). Here, we vary the control freedom K and system size N , and repeat the simulation 10 times with random control fields $u_k(t)$ or $s_k(t)$ for average performance. The PWM method outperforms the default method for $N \leq 4$, $K \lesssim 10$ and $N \geq 5$, $K \lesssim 5$, which is qualitatively consistent with the FLOP analysis. Over

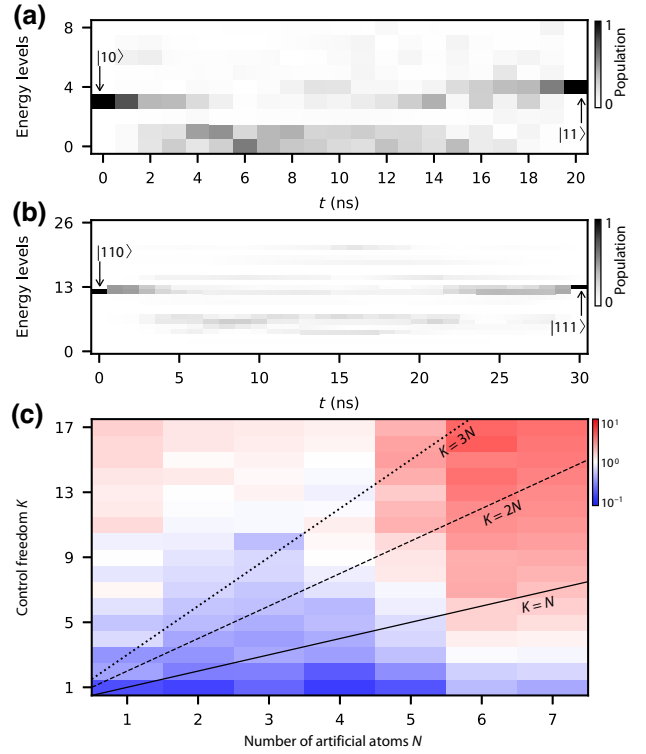


FIG. 5. (a) The dynamics of the system during a CNOT gate, where the population of $|10\rangle$ is transferred to $|11\rangle$ with 0.9999 fidelity. (b) The dynamics of the system during a CCNOT gate, where the population of $|110\rangle$ is transferred to $|111\rangle$ with 0.9999 fidelity. (c) Comparison of the computational resources γ between the PWM and the conventional approaches for solving TDSE. The former outperforms the latter for a relatively small control freedom, $K \lesssim 5-10$, which is consistent with the FLOP analysis.

the simulated parameter regime, the two corresponding numerical time consumptions achieve a minimum ratio of $\gamma = 0.17$ at $N = 4$, $K = 1$, and a maximum of 4.36 at $N = 6$, $K = 16$. The average value below $K = 5$ (included) is 0.57, which indicates a significant acceleration of the numerical calculation.

When considering a finite frequency cutoff, $\Omega_f/2\pi$, to the designed control fields $u_k(t)$ and $s_k(t)$, the filtered result may have an arbitrary waveform $u'_k(t)$. It has an infinitely large bandwidth by definition, where all the frequency components above $\Omega_f/2\pi$ should be strictly zero. In this regard, the sampling time of the control field τ may become too coarse to simulate the TDSE with the filtered fields. In practice, one may choose a finer time step, $\tau' \ll 2\pi/\Omega_f$, to simulate the control performance of $u'_k(t)$. Here, the same value of τ' can be used to generate a PWM sequence $s'_k(t)$ to accelerate the simulation process. The numerical advantage remains the same as shown in Fig. 5(c).

C. Cryogenic implementation

Towards building a scalable controller for SQC, we anticipate that arrays of PWM controllers can be integrated at low temperature with current cryogenic CMOS (cryo-CMOS) [28–35] or RSFQ technologies [62–65]. They have a typical switching speed of about 100 ps and about 1 ps, respectively. Both technologies enable the relocation of the controller to the cryogenic environment, which avoids racks of room-temperature electronics and substantially reduces the need for lossy and noisy cables connecting the controller and the quantum processor. One may either mix a relatively slow pulse sequence generated by the cryo-CMOS switch with a fast oscillating carrier wave, or generate a sequence of rapid PWM pulses directly with RSFQ switches. Compared with a cryogenic AWG, where tens of cryo-CMOS switches are superimposed to generate an arbitrary waveform, the PWM controller requires only a single switch for each degree of control freedom and thus leads to a dramatic reduction of the hardware demands. Compared with the existing RSFQ approach [48–52], the PWM pulses naturally have a finite width. It thus indicates a slower switching rate rather than generating a sequence of RSFQ pulses of about 2-ps width. The number of switching events is also substantially smaller than the RSFQ approach.

V. CONCLUSIONS AND OUTLOOK

We apply the concept of PWM to quantum systems, and propose the PWM method that enables arbitrary control of a general quantum system with a sequence of simple pulses. The performance of the pulse train can be efficiently evaluated by a matrix decomposition method, which avoids numerically expensive matrix exponentials and accelerates the TDSE solver for a relatively small number of controls. The control protocol is resilient to time jitter, switching delay, and leakage. We anticipate that the implementations of a PWM controller may be achieved with existing semiconductor or superconductor technologies, but with a lower demand of hardware resources than other controllers, such as AWG and RSFQ. These results indicate a simple, precise, robust, and scalable control protocol for a general quantum system. Together with the advances of high-density wiring and packaging techniques, an experimental realization of the PWM controller at cryogenic temperature may offer significant advances for building a practically useful quantum information processor.

Besides achieving high fidelity, one further goal in QOC is to implement the controls as fast as possible. Recent experiments have demonstrated that, in spin systems, the time-optimal control fields may converge to a pulse sequence form when T approaches its theoretical minimum value [70–72]. This observation indicates that a pulse train might be a more suitable and natural choice than

a continuous waveform for solving quantum time-optimal control problems. We anticipate that the PWM method may open up alternative ways for seeking time-optimal control pulses in a general quantum system.

The codes that support the findings of this study are available online [73].

ACKNOWLEDGMENTS

We thank Benjamin Lienhard, Olli-Pentti Saira, Visa Vesterinen, and Mikko Möttönen for insightful discussions. Q.C. acknowledges support from the Technology Industries of Finland Centennial Foundation and the Jane and Aatos Erkko Foundation through the Future Makers program. R.W. acknowledges support from the National Natural Science Foundation of China (Grants No. 62173201 and No. 61833010). H.R. acknowledges support from the U.S. Army Research Office (Grant No. W911NF-19-1-0382).

APPENDIX A: WAVEFORM-PULSE TRAIN CORRESPONDENCE

1. Single-frequency waveform

To demonstrate the equivalence between a waveform and a pulse train, we start from the simplest case where the former is a sinusoidal function of time, $u_1(t) = \sin(\omega t + \phi)$. Here, the subscript $k = 1$ is a special case of the k th control field in a general quantum control system. We describe the corresponding pulse train as a sequence of rectangular pulses centered at $(m - 1/2)\tau$ for $m = 1, \dots, M$,

$$s_1(t) = \xi_1 \sum_{m=1}^M \left\{ \theta \left[t - \left(m - \frac{1}{2} \right) \tau + \frac{\tau_{1,m}}{2} \right] - \theta \left[t - \left(m - \frac{1}{2} \right) \tau - \frac{\tau_{1,m}}{2} \right] \right\}. \quad (\text{A1})$$

Here, $\theta(t)$ is the unit step function, $M = T/\tau$ is the number of pulses in one period $T = 2\pi/\omega$, ξ_1 is the magnitude for all the pulses, and $|\tau_{1,m}|$ is the width of the m th pulse. By utilizing a Fourier series, the above equation can be equivalently written as

$$s_1(t) = \frac{\xi_1}{T} \sum_{m=1}^M \tau_{1,m} + \sum_{n \neq 0} \left[\sum_{m=1}^M \frac{\xi_1}{n\pi} \sin \left(\frac{\tau_{1,m} n\pi}{\tau} \right) e^{-in\omega(m-1/2)\tau} \right] e^{in\omega t}. \quad (\text{A2})$$

Moreover, we define the signed pulse width and magnitude of the m th pulse as

$$\begin{aligned}\tau_{1,m} &= \frac{1}{\xi_1} \int_{(m-1)\tau}^{m\tau} dt \sin(\omega t + \phi), \\ \xi_1 &= \max_{0 \leq t \leq T} |\sin(\omega t + \phi)|.\end{aligned}\quad (\text{A3})$$

This definition guarantees that the pulse width $|\tau_{1,m}|$ is always smaller than or equal to τ , while its \pm sign determines the polarization of the pulse.

By inserting Eq. (A3) into Eq. (A2), we can readily eliminate the first term in the Fourier series that is the dc component. For the second term, we use the following approximation to simplify the summation:

$$\begin{aligned}\sum_{n \ll M} \left[\sum_{m=1}^M \frac{\xi_1}{n\pi} \sin\left(\frac{\tau_{1,m}}{\tau} \cdot \frac{n\pi}{M}\right) e^{-in\omega(m-1/2)\tau} \right] e^{in\omega t} \\ \approx \sum_{n \ll M} \left[\sum_{m=1}^M \frac{\xi_1 \tau_{1,m}}{M\tau} e^{-in\omega(m-1/2)\tau} \right] e^{in\omega t}.\end{aligned}\quad (\text{A4})$$

In general, this expression holds for $n \ll M$. However, it is reasonably precise for all values of n if we assume that $M \gg 1$. This conclusion arises because the coefficient $1/n$ becomes sufficiently small in this case and plays a negligibly small contribution to the summation. In this regard, we simplify Eq. (A2) as

$$s_1(t) = \sum_{n \neq 0} \left[\sum_{m=1}^M \frac{\xi_1 \tau_{1,m}}{M\tau} e^{-in\omega(m-1/2)\tau} \right] e^{in\omega t}.\quad (\text{A5})$$

For $n = 1$ in the summation, we have

$$\begin{aligned}\frac{\xi_1}{M} \sum_{m=1}^M \frac{\tau_{1,m}}{\tau} e^{-i\omega(m-1/2)\tau} e^{i\omega t} \\ = \frac{e^{i\pi/M}}{4\pi} \left[M(1 - e^{i2\pi/M}) e^{i\phi} \right. \\ \left. + (1 - e^{-i2\pi/M}) e^{-i\phi} \sum_{m=1}^M e^{-i(2m/M)2\pi} \right] e^{i\omega t} \approx \frac{e^{i(\omega t + \phi)}}{2i}.\end{aligned}\quad (\text{A6})$$

Similarly, for $n = -1$, we have

$$\begin{aligned}\frac{\xi_1}{M} \sum_{m=1}^M \frac{\tau_{1,m}}{\tau} e^{i\omega(m-1/2)\tau} e^{-i\omega t} \\ = \frac{e^{-i\pi/M}}{4\pi} \left[(1 - e^{i2\pi/M}) e^{i\phi} \sum_{m=1}^M e^{i(2m/M)2\pi} \right. \\ \left. + M(1 - e^{-i2\pi/M}) e^{-i\phi} \right] e^{-i\omega t} \approx -\frac{e^{i(\omega t - \phi)}}{2i}.\end{aligned}\quad (\text{A7})$$

One can verify that all the other terms, from $n = \pm 2$ to $\pm(M-2)$, are equal to *zero*. This observation shows that the pulse sequence $s_1(t)$ can be regarded as a combination of $u_1(t)$ and a high-frequency error term. The frequency threshold is $\Omega_1 = (M-1)\omega \approx M\omega$, below which the Fourier components of the pulse sequence $s_1(t)$ and the waveform $u_1(t)$ are indistinguishable from each other. The error exists only in high-frequency components, which can be reasonably omitted by the same argument behind the rotating-wave approximation, or physically filtered before the sample input in experiments. We note that the value of Ω_1 is fully determined by the pulse number M , which indicates the ability to adjust the scale of the approximation error for different purposes.

2. Arbitrary waveform

We now study the general case where $u_1(t)$ is an arbitrary real function. We assume that the waveform has a finite frequency bandwidth $[\omega_{\min}, \omega_{\max}]$, and write it as

$$u_1(t) = 2 \int_{\omega_{\min}}^{\omega_{\max}} d\omega |U_1(\omega)| \sin(\omega t + \phi(\omega)),\quad (\text{A8})$$

where $U_1(\omega)$ is the Fourier transform of $u_1(t)$, and $\phi(\omega) = \arctan(-\text{Re}[U_1(\omega)]/\text{Im}[U_1(\omega)])$. Here, we have used the property that $U_1(-\omega) = U_1^*(\omega)$ for the real function $u_1(t)$.

Following the developments in the single-frequency case, for each frequency component ω , one can generate a sequence of PWM pulses to approximate the sinusoidal component $\sin(\omega t + \phi(\omega))$. In each short time interval, the signed pulse width $\tau_{1,m}(\omega)$ is defined in the same way as in Eq. (A3). We further require that the signed pulse widths for different frequencies must be the same, which is achieved by adjusting the pulse magnitudes $\xi_1(\omega)$ for different frequencies. Assuming that the desired value of the signed pulse width is $\tau_{1,m}$, the pulse magnitude corresponding to the frequency ω should be calculated as

$$\xi_1(\omega) = \frac{2}{\tau_{1,m}} \int_{(m-1)\tau}^{m\tau} dt U_1(\omega) \sin(\omega t + \phi(\omega)).\quad (\text{A9})$$

The pulse magnitude ξ_1 in the m th time interval is an integral of $\xi_1(\omega)$ over the entire frequency range $[\omega_{\min}, \omega_{\max}]$,

$$\begin{aligned}\xi_1 &= \frac{2}{\tau_{1,m}} \int_{(m-1)\tau}^{m\tau} dt \int_{\omega_{\min}}^{\omega_{\max}} d\omega U_1(\omega) \sin(\omega t + \phi(\omega)) \\ &= \frac{1}{\tau_{1,m}} \int_{(m-1)\tau}^{m\tau} dt u_1(t).\end{aligned}\quad (\text{A10})$$

From a different perspective, if we require the pulse magnitude to be ξ_1 , the corresponding signed pulse width

is

$$\tau_{1,m} = \frac{1}{\xi_1} \int_{(m-1)\tau}^{m\tau} dt u_1(t). \quad (\text{A11})$$

This means that an arbitrary function $u_1(t)$ with finite frequency range can also be approximated with a pulse train by neglecting high-frequency errors above Ω_1 . One can prove that the threshold frequency in this case is $\Omega_1 \approx M\omega_{\min}$. So long as $\Omega_1 \gg \omega_{\max}$, or, equivalently, $\tau \ll 2\pi/\omega_{\max}$, the pulse sequence $s_1(t)$ is indistinguishable from $u_1(t)$ below Ω_1 .

APPENDIX B: ERROR ANALYSIS

We consider a general quantum system described by the Hamiltonian

$$H = H_0 + \sum_{k=1}^K u_k(t)H_k, \quad (\text{B1})$$

where H_k is Hermitian and $u_k(t)$ is a real function of time. The system with PWM control can be described as

$$H = H_0 + \sum_{k=1}^K s_k(t)H_k. \quad (\text{B2})$$

We now compare the time propagation of the system driven by the waveforms $u_k(t)$ and by the pulse trains $s_k(t)$.

1. Single-control case

We start from the simplest case with $K = 1$. The time propagator with waveform $u_1(t)$ in the m th time interval can be written in a Dyson series as

$$U_u[m\tau, (m-1)\tau] = 1 - i \sum_{k_1=0}^1 H_{k_1} \int_{(m-1)\tau}^{m\tau} dt u_{k_1}(t) + (-i)^2 \sum_{k_1, k_2=0}^1 \left[H_{k_1} H_{k_2} \int_{(m-1)\tau}^{m\tau} dt_1 \int_{(m-1)\tau}^{t_1} dt_2 u_{k_1}(t_1) u_{k_2}(t_2) \right] + O(\tau^3), \quad (\text{B3})$$

where we have defined $u_0(t) \equiv 1$ to simplify the notation. On the other hand, the corresponding pulsed time propagator can be written as

$$U_s[m\tau, (m-1)\tau] = \exp(-i|\tau_{0,m}|H_0) \exp(-i|\tau_{1,m}|(H_0 + \text{sgn}[\tau_{1,m}]\xi_1 H_1)) \exp(-i|\tau_{0,m}|H_0), \quad (\text{B4})$$

where $\tau_{1,m} = \int_{(m-1)\tau}^{m\tau} dt u_1(t)/\xi_1$, $\tau_{0,m} = (\tau - |\tau_{1,m}|)/2$. Because the generators of time propagation are time independent, one can simply use a Taylor series to rewrite the propagator as

$$U_s[m\tau, (m-1)\tau] = \left[1 - i|\tau_{0,m}|H_0 + \frac{(-i)^2}{2!} (|\tau_{0,m}|H_0)^2 + O(\tau^3) \right] \times \left[1 - i|\tau_{1,m}|(H_0 + \text{sgn}[\tau_{1,m}]\xi_1 H_1) + \frac{(-i)^2}{2!} (|\tau_{1,m}|(H_0 + \text{sgn}[\tau_{1,m}]\xi_1 H_1))^2 + O(\tau^3) \right] \times \left[1 - i|\tau_{0,m}|H_0 + \frac{(-i)^2}{2!} (|\tau_{0,m}|H_0)^2 + O(\tau^3) \right] = 1 - i(\tau H_0 + \xi_1 \tau_{1,m} H_1) + \frac{(-i)^2}{2!} (\tau H_0 + \xi_1 \tau_{1,m} H_1)^2 + O(\tau^3). \quad (\text{B5})$$

We define the propagation error as the difference between the two evolution operators

$$\delta U[m\tau, (m-1)\tau] = U_u[m\tau, (m-1)\tau] - U_s[m\tau, (m-1)\tau] = (-i)^2 \sum_{k_1, k_2=0}^1 H_{k_1} H_{k_2} \left(\int_{(m-1)\tau}^{m\tau} dt_1 \int_{(m-1)\tau}^{t_1} dt_2 u_{k_1}(t_1) u_{k_2}(t_2) - \frac{1}{2!} \int_{(m-1)\tau}^{m\tau} dt_1 u_{k_1}(t_1) \int_{(m-1)\tau}^{m\tau} dt_2 u_{k_2}(t_2) \right) + O(\tau^3). \quad (\text{B6})$$

To simplify the time-ordered integral in the above equation, we use the relations

$$\int_{(m-1)\tau}^{m\tau} dt u_k(t) = u_k(t')\tau + \frac{1}{2!}u'_k(t')\tau^2 + O(\tau^3), \tag{B7}$$

$$\int_{(m-1)\tau}^{m\tau} dt_1 \int_{(m-1)\tau}^{t_1} dt_2 u_{k_1}(t_1)u_{k_2}(t_2) = \frac{1}{2}u_{k_1}(t')u_{k_2}(t')\tau^2 + O(\tau^3). \tag{B8}$$

Here, t' is an arbitrary time instance within $[(m - 1)\tau, m\tau]$. By inserting Eqs. (B8) and (B7) into Eq. (B6), we obtain $\delta U[m\tau, (m - 1)\tau] = O(\tau^3)$. This result shows that the pulse propagation has second-order accuracy in simulating the dynamics driven by a continuous waveform.

2. Multicontrol case

For a general quantum system with K controls, the pulse time propagation is

$$\begin{aligned} U_s[m\tau, (m - 1)\tau] &= \exp(-i|\tau_{0,m}|H_0) \exp[-i|\tau_{1,m}|(H_0 + \text{sgn}[\tau_{1,m}]\xi_1 H_1)] \times \dots \\ &\times \exp\left[-i|\tau_{K,m}|\left(H_0 + \sum_{k=1}^K \text{sgn}[\tau_{k,m}]\xi_k H_k\right)\right] \\ &\times \exp\left[-i|\tau_{(K-1),m}|\left(H_0 + \sum_{k=1}^{K-1} \text{sgn}[\tau_{k,m}]\xi_k H_k\right)\right] \times \dots \exp(-i|\tau_{0,m}|H_0), \end{aligned} \tag{B9}$$

where

$$|\tau_{k,m}| = \begin{cases} \frac{1}{2}\left[\tau - \frac{1}{\xi_1}\left|\int_{(m-1)\tau}^{m\tau} dt u_1(t)\right|\right] & \text{for } k = 0, \\ \frac{1}{2}\left[\frac{1}{\xi_k}\left|\int_{(m-1)\tau}^{m\tau} dt u_k(t)\right| - \frac{1}{\xi_{k+1}}\left|\int_{(m-1)\tau}^{m\tau} dt u_{(k+1)}(t)\right|\right] & \text{for } 1 \leq k \leq K - 1, \\ \frac{1}{\xi_K}\left|\int_{(m-1)\tau}^{m\tau} dt u_K(t)\right| & \text{for } k = K. \end{cases} \tag{B10}$$

Here, to simplify the notation, we have relabeled the control fields such that $|\tau| > |\tau_{1,m}| > \dots > |\tau_{K,m}|$. We note that the \pm sign of $\tau_{k,m}$ is determined by the \pm sign of the integral $\int_{(m-1)\tau}^{m\tau} dt u_k(t)$ only. The physical meaning is that we align all the pulses for different k to the same center of each time interval. Thus, the interaction $\text{sgn}[\tau_{k,m}]\xi_k H_k$ with larger pulse area is turned on earlier and turned off later compared with the others. Following the same procedure in the single-control case, we use the Taylor series to rewrite each exponential to second order and recombine the terms according to τ . One can prove that the pulse propagation is still second-order accurate for $K > 1$. This result is as precise as the staircase approximation of an arbitrary function, which is widely used in numerical simulations and is utilized by an arbitrary waveform generator.

APPENDIX C: NUMERICAL EFFICIENCY

In numerical simulation, the replacement $u_k(t) \rightarrow s_k(t)$ has an advantage that the resulting generator of time propagation belongs to a finite set $H(t) \in \{H_0, H_0 + \xi_1 H_1, H_0 - \xi_1 H_1, \dots, H_0 + \dots + \xi_K H_K, \dots, H_0 - \dots - \xi_K H_K\}$. This observation indicates that the numerically expensive calculation of matrix exponents in conventional design efforts can be circumvented with diagonal matrix exponents instead. In detail, the pulse time propagation can be written as

$$\begin{aligned} U_s[m\tau, (m - 1)\tau] &= P_0 \exp\left[-i\left(\tau - \frac{|\tau_{1,m}|}{2}\right)\Lambda_0\right] P_0^\dagger P_1 \exp[-i|\tau_{1,m}|\Lambda_1] P_1^\dagger \times \dots \\ &\times P_K \exp[-i|\tau_{K,m}|\Lambda_K] P_K^\dagger P_{K-1} \exp[-i|\tau_{K-1,m}|\Lambda_{K-1}] P_{K-1}^\dagger \times \dots \\ &\times P_0 \exp\left[-i\left(\tau - \frac{|\tau_{1,m}|}{2}\right)\Lambda_0\right] P_0^\dagger. \end{aligned} \tag{C1}$$

Here, Λ_k and P_k are real diagonal and unitary matrices, respectively. For $k=0$, it is defined as $H_0 = P_0 \Lambda_0 P_0^\dagger$. However, the calculation of Λ_k for $k=1, 2, \dots, K$ depends on the polarization of $s_k(t)$. For example, if the integrals of the control fields are $\tau_{1,m} < 0$, $\tau_{2,m} < 0$, and $\tau_{3,m} \geq 0$ in the m th interval, we have $H_0 - \xi_1 H_1 = P_1 \Lambda_1 P_1^\dagger$, $H_0 - \xi_1 H_1 - \xi_2 H_2 = P_2 \Lambda_2 P_2^\dagger$, $H_0 - \xi_1 H_1 - \xi_2 H_2 + \xi_3 H_3 = P_3 \Lambda_3 P_3^\dagger$. Thus, one has to determine the polarization of $s_k(m)$ before calculating the propagator. Because the set is finite, one can diagonalize different terms in advance and save the result. This procedure is particularly efficient in PYTHON by using its dictionary function. In comparison, the time propagation with the control field $u_1(t)$ is

$$U_u(T, 0) = \prod_{m=1}^M \exp \left[-i\tau \left(H_0 + \sum_{k=1}^K u_k(m\tau) H_k \right) \right]. \quad (\text{C2})$$

Here, the value of $u_k(t)$ can be arbitrary such that the generator of time propagation consists of a convex set $\{H_0 + \sum_k u_k(t) H_k \mid t \in [0, T]\}$. One cannot simply diagonalize the generators, and thus matrix exponentials are unavoidable.

In Fig. 2(c) of the main text, we compare the numerical efficiency of the two approaches in simulating a d -dimensional system. The calculation is carried out under PYTHON 3.7.3 on Windows 10 64-bit (3.20 GHz Intel® Core™ i7-8700, 16 GB). The computational time is measured by using the `perf_counter()` command in the `time` package, and the matrix product is calculated by the `@` operator. The default method for calculating the matrix exponential refers to the `linalg.expm()` command in the `scipy` package, which is based on the scaling and squaring method [57]. We observe that a MATLAB® implementation of the PWM method seems to be less efficient than PYTHON, which we attribute to the possibly lower efficiency of its dictionary function. In the future, even higher-numerical advantages may be achieved by using JIT (just-in-time compiling), CYTHON

(C extension in PYTHON), cuda (GPU processing), and TensorFlow.

APPENDIX D: GENERALIZATIONS

1. n -level PWM

In Appendices A and B, we defined the pulse magnitude of the pulse train as a constant, ξ_k . The polarization of the pulse is determined by the short-time integral of $u_k(t)$, i.e., the sign of $\tau_{k,m}$ defined in Eq. (A11). This is called the 3-level PWM in the literature of power electronics as the field at any time instance is chosen from three candidate values [37]. Besides, there are many other forms of PWM, among which the 2-level PWM is widely used in classical control systems [37]. Different from the 3-level case, the 2-level PWM approximates an arbitrary function by switching between two states, as shown in Fig. 6(a). If we define the two possible magnitudes as ξ_k and $\xi_{k'}$, the time durations in each state, $\tau_{k,m}$ and $\tau_{k',m}$, satisfy the relation

$$\xi_k \tau_{k,m} + \xi_{k'} \tau_{k',m} = \int_{(m-1)\tau}^{m\tau} dt u_k(t), \quad (\text{D1})$$

where $\tau_{k,m} + \tau_{k',m} = \tau$. One can follow the same procedure in Appendices A and B, and prove that the 2-level PWM pulse sequences can also achieve full control of a quantum system.

2. Choice of magnitude

In Appendices A and B, we defined the pulse magnitude as $\xi_k = \max |u_k(t)|$, $t \in [0, T]$, which is the maximum value of the waveform over the entire control time. However, the magnitude can also be larger. The extreme case is achieved when the pulse magnitude approaches infinity, $\xi_k \rightarrow \infty$, indicating the so-called hard pulse. Correspondingly, the pulse width should be shrunk by the same factor to fulfill the requirement of Eq. (A11). This extreme case describes a sequence of instantaneous kicks to the system, and the corresponding evolution operator is (assuming that all the pulses are positive)

$$U_s[m\tau, (m-1)\tau] = \exp(-i\tau H_0/2) \exp(-i\tau_{1,m} \xi_1 H_1/2) \cdots \exp(-i\tau_{K,m} \xi_K H_K/2) \\ \times \exp(-i\tau_{K,m} \xi_K H_K/2) \cdots \exp(-i\tau_{1,m} \xi_1 H_1/2) \exp(-i\tau H_0/2). \quad (\text{D2})$$

The advantage of choosing an arbitrarily large magnitude is that the number of generators of time propagation is reduced from $(2^K - K)$ to $(K + 1)$, which simplifies the numerical simulation. However, as can be seen from the Fourier analysis in Eq. (A5), the scale of the high-frequency errors depends on the pulse magnitude. Thus, the simulation accuracy will be slightly lower than with the default PWM sequence. In addition, a physical

implementation of such intensive pulses may lead to less favorable control fidelities owing to the power limit of real devices.

3. Gaussian pulses

In Appendices A and B, we defined the pulses to be perfect rectangular. However, in real implementations one

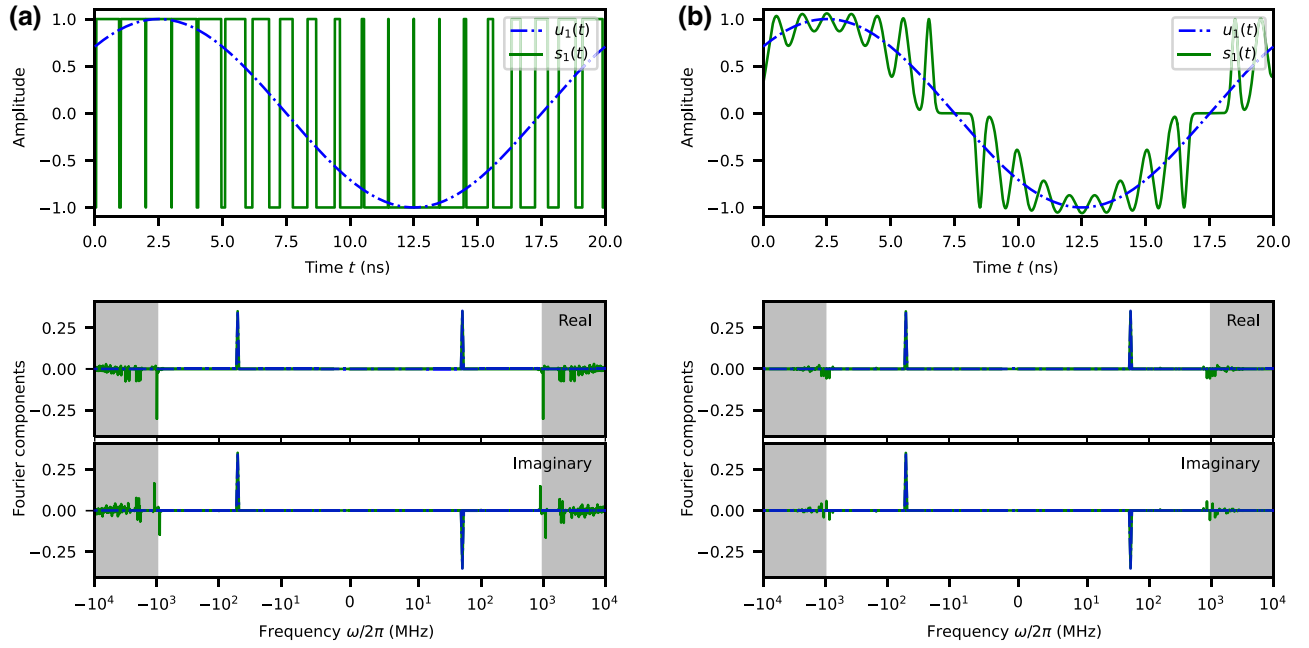


FIG. 6. (a) Two-level and (b) Gaussian PWM sequences, respectively. The frequency threshold $\Omega_1 \approx M\omega_{\min}$ is set as $M = 20$ times the minimum frequency of $u_1(t)$, i.e., $\Omega_1/2\pi \approx 1$ GHz. The frequency components between the maximum frequency of $u_1(t)$ and Ω_1 are, in principle, entirely suppressed by properly designed PWM pulses with $\Omega_1 \gg \omega_{\max}$. The difference between $u_1(t)$ and $s_1(t)$ exists only above Ω_1 (gray area).

may expect to use a sequence of smooth pulses instead, considering the power and bandwidth specifications of real control protocols. Here, we consider a sequence of Gaussian pulses, as shown in Fig. 6(b), which is described as

$$s_k(t) = \xi_k \sum_{m=1}^M e^{-\pi[t-(m-1/2)\tau]/\tau_{k,m}}. \quad (\text{D3})$$

It can also be rewritten as follows by using the Fourier series:

$$s_k(t) = \sum_{n=-\infty}^{+\infty} \left(\frac{\xi_k}{T} \sum_{m=1}^M \tau_{k,m} e^{-\pi(n\omega t)^2/4\pi} e^{-in\omega(m-1/2)\tau} \right) e^{in\omega t}. \quad (\text{D4})$$

Following the same analyses as in Appendix A, one can prove that the Fourier components of $u_k(t)$ and $s_k(t)$ are exactly the same below the threshold $\Omega_k \approx M\omega_{\min}$, as long as

$$\tau_{k,m} = \frac{1}{\xi_k} \int_{(m-1)\tau}^{m\tau} dt u_k(t). \quad (\text{D5})$$

This is exactly the same definition of the signed pulse width for default rectangular PWM pulses, i.e., Eq. (A11).

4. Higher-order expansion

In Appendices A and B, we proved that the PWM pulse sequence $s_k(t)$ is a second-order accurate approximation for simulating the time propagation driven by $u_k(t)$. This result is based on the assumption that there exists only one pulse in each time interval. To achieve higher-order accuracy in time propagation, one can follow the same procedure introduced in Refs. [45–47], and insert more pulses in each time interval. We write the exact short-time propagation of $u_k(t)$ as

$$U_u[m\tau, (m-1)\tau] = S_2^{(m)}(\tau) + C_3^{(m)}\tau^3 + O(\tau^4), \quad (\text{D6})$$

where $S_2^{(m)}(\tau) = U_s[m\tau, (m-1)\tau]$ is the time propagation driven by PWM pulses, i.e., Eq. (B4). On the other hand, the exact evolution can also be written as

$$\begin{aligned} U_u[m\tau, (m-1)\tau] &= U_{\{u_k\}}[m\tau, (m-s)\tau] \\ &\quad \times U_{\{u_k\}}[(m-s)\tau, (m-1+s)\tau] \\ &\quad \times U_{\{u_k\}}[(m-1+s)\tau, (m-1)\tau]. \end{aligned} \quad (\text{D7})$$

Combining Eqs. (D6) and (D7), we have

$$\begin{aligned}
 U_u[m\tau, (m-1)\tau] &= [S_2^{(m)}(s\tau) + C_3^{(m)}s^3\tau^3 + O(\tau^4)] \\
 &\quad \times [S_2^{(m)}[(1-2s)\tau] + C_3^{(m)}(1-2s)^3\tau^3 + O(\tau^4)] \\
 &\quad \times [S_2^{(m)}(s\tau) + C_3^{(m)}s^3\tau^3 + O(\tau^4)] \\
 &= S_2^{(m)}(s\tau)S_2^{(m)}[(1-2s)\tau]S_2^{(m)}(s\tau) \\
 &\quad + C_3^{(m)}\tau^3[2s^3 + (1-2s)^3] + O(\tau^4). \quad (D8)
 \end{aligned}$$

When $2s^3 + (1-2s)^3 = 0$, we obtain the PWM sequence with third-order accuracy

$$U_s[m\tau, (m-1)\tau] = S_3^{(m)}(\tau) = U_{\{u_1\},m} + O(\tau^4), \quad (D9)$$

where

$$S_3^{(m)}(\tau) = S_2^{(m)}(s\tau)S_2^{(m)}[(1-2s)\tau]S_2^{(m)}(s\tau). \quad (D10)$$

Similarly, one can obtain an arbitrarily high-order form of PWM. We note that, although the solution for s always exists mathematically, the value of s may not be positive and real in higher-order expansions. The propagator $S_n^{(m)}(\tau)$ in such cases cannot be physically implemented because the polarization of the drift Hamiltonian H_0 is not controllable. However, one can prove that there is always a real and positive solution $s = 1/(2 - 2^{1/(2n+1)})$ for the $(2n+1)$ th-order form of PWM, $S_{2n+1}^{(m)}(\tau)$ [45–47].

-
- [1] W. S. Warren, H. Rabitz, and M. Dahleh, Coherent control of quantum dynamics: The dream is alive, *Science* **259**, 1581 (1993).
- [2] H. Rabitz, R. de Vivie-Riedle, M. Motzkus, and K. Kompa, Whither the future of controlling quantum phenomena?, *Science* **288**, 824 (2000).
- [3] A. P. Peirce, M. A. Dahleh, and H. Rabitz, Optimal control of quantum-mechanical systems: Existence, numerical approximation, and applications, *Phys. Rev. A* **37**, 4950 (1988).
- [4] R. Kosloff, S. Rice, P. Gaspard, S. Tersigni, and D. Tanner, Wavepacket dancing: Achieving chemical selectivity by shaping light pulses, *Chem. Phys.* **139**, 201 (1989).
- [5] R. S. Judson and H. Rabitz, Teaching lasers to control molecules, *Phys. Rev. Lett.* **68**, 1500 (1992).
- [6] A. Assion, T. Baumert, M. Bergt, T. Brixner, B. Kiefer, V. Seyfried, M. Strehle, and G. Gerber, Control of chemical reactions by feedback-optimized phase-shaped femtosecond laser pulses, *Science* **282**, 919 (1998).
- [7] L. Tian and S. Lloyd, Resonant cancellation of off-resonant effects in a multilevel qubit, *Phys. Rev. A* **62**, 050301 (2000).
- [8] M. Steffen, J. M. Martinis, and I. L. Chuang, Accurate control of Josephson phase qubits, *Phys. Rev. B* **68**, 224518 (2003).
- [9] F. Motzoi, J. M. Gambetta, P. Rebentrost, and F. K. Wilhelm, Simple pulses for elimination of leakage in weakly nonlinear qubits, *Phys. Rev. Lett.* **103**, 110501 (2009).
- [10] S. Safaei, S. Montangero, F. Taddei, and R. Fazio, Optimized single-qubit gates for Josephson phase qubits, *Phys. Rev. B* **79**, 064524 (2009).
- [11] P. Rebentrost and F. K. Wilhelm, Optimal control of a leaking qubit, *Phys. Rev. B* **79**, 060507 (2009).
- [12] R. Schutjens, F. A. Dagga, D. J. Egger, and F. K. Wilhelm, Single-qubit gates in frequency-crowded transmon systems, *Phys. Rev. A* **88**, 052330 (2013).
- [13] E. Zahedinejad, J. Ghosh, and B. C. Sanders, High-fidelity single-shot Toffoli gate via quantum control, *Phys. Rev. Lett.* **114**, 200502 (2015).
- [14] J. M. Chow, L. DiCarlo, J. M. Gambetta, F. Motzoi, L. Frunzio, S. M. Girvin, and R. J. Schoelkopf, Optimized driving of superconducting artificial atoms for improved single-qubit gates, *Phys. Rev. A* **82**, 040305 (2010).
- [15] J. M. Chow, A. D. Córcoles, J. M. Gambetta, C. Rigetti, B. R. Johnson, J. A. Smolin, J. R. Rozen, G. A. Keefe, M. B. Rothwell, M. B. Ketchen, and M. Steffen, Simple all-microwave entangling gate for fixed-frequency superconducting qubits, *Phys. Rev. Lett.* **107**, 080502 (2011).
- [16] J. M. Chow, J. M. Gambetta, A. D. Córcoles, S. T. Merkel, J. A. Smolin, C. Rigetti, S. Poletto, G. A. Keefe, M. B. Rothwell, J. R. Rozen, M. B. Ketchen, and M. Steffen, Universal quantum gate set approaching fault-tolerant thresholds with superconducting qubits, *Phys. Rev. Lett.* **109**, 060501 (2012).
- [17] R. W. Heeres, P. Reinhold, N. Ofek, L. Frunzio, L. Jiang, M. H. Devoret, and R. J. Schoelkopf, Implementing a universal gate set on a logical qubit encoded in an oscillator, *Nat. Commun.* **8**, 94 (2017).
- [18] A. Galiatdinov, A. N. Korotkov, and J. M. Martinis, Resonator-zero-qubit architecture for superconducting qubits, *Phys. Rev. A* **85**, 042321 (2012).
- [19] J. Ghosh, A. Galiatdinov, Z. Zhou, A. N. Korotkov, J. M. Martinis, and M. R. Geller, High-fidelity controlled- σ^z gate for resonator-based superconducting quantum computers, *Phys. Rev. A* **87**, 022309 (2013).
- [20] R. Barends, *et al.*, Superconducting quantum circuits at the surface code threshold for fault tolerance, *Nature* **508**, 500 (2014).
- [21] J. Kelly, *et al.*, State preservation by repetitive error detection in a superconducting quantum circuit, *Nature* **519**, 66 (2015).
- [22] P. Roushan, *et al.*, Spectroscopic signatures of localization with interacting photons in superconducting qubits, *Science* **358**, 1175 (2017).
- [23] E. Lucero, M. Hofheinz, M. Ansmann, R. C. Bialczak, N. Katz, M. Neeley, A. D. O’Connell, H. Wang, A. N. Cleland, and J. M. Martinis, High-fidelity gates in a single Josephson qubit, *Phys. Rev. Lett.* **100**, 247001 (2008).
- [24] J. Kelly, *et al.*, Optimal quantum control using randomized benchmarking, *Phys. Rev. Lett.* **112**, 240504 (2014).
- [25] F. Arute, *et al.*, Quantum supremacy using a programmable superconducting processor, *Nature* **574**, 505 (2019).
- [26] B. Foxen, *et al.*, (Google AI Quantum) Demonstrating a continuous set of two-qubit gates for near-term quantum algorithms, *Phys. Rev. Lett.* **125**, 120504 (2020).

- [27] M. P. Harrigan, *et al.*, Quantum approximate optimization of non-planar graph problems on a planar superconducting processor, *Nat. Phys.* **17**, 332 (2021).
- [28] J. M. Hornibrook, J. I. Colless, I. D. Conway Lamb, S. J. Pauka, H. Lu, A. C. Gossard, J. D. Watson, G. C. Gardner, S. Fallahi, M. J. Manfra, and D. J. Reilly, Cryogenic control architecture for large-scale quantum computing, *Phys. Rev. Appl.* **3**, 024010 (2015).
- [29] D. J. Reilly, Engineering the quantum-classical interface of solid-state qubits, *npj Quantum Inf.* **1**, 15011 (2015).
- [30] L. M. K. Vandersypen, H. Bluhm, J. S. Clarke, A. S. Dzurak, R. Ishihara, A. Morello, D. J. Reilly, L. R. Schreiber, and M. Veldhorst, Interfacing spin qubits in quantum dots and donors—hot, dense, and coherent, *npj Quantum Inf.* **3**, 34 (2017).
- [31] J. C. Bardin, *et al.*, Design and characterization of a 28-nm bulk-CMOS cryogenic quantum controller dissipating less than 2 mW at 3 K, *IEEE J. Solid-State Circuits* **54**, 3043 (2019).
- [32] J. van Dijk, E. Kawakami, R. Schouten, M. Veldhorst, L. Vandersypen, M. Babaie, E. Charbon, and F. Sebastiano, Impact of classical control electronics on qubit fidelity, *Phys. Rev. Appl.* **12**, 044054 (2019).
- [33] L. Petit, H. G. J. Eenink, M. Russ, W. I. L. Lawrie, N. W. Hendrickx, S. G. J. Philips, J. S. Clarke, L. M. K. Vandersypen, and M. Veldhorst, Universal quantum logic in hot silicon qubits, *Nature* **580**, 355 (2020).
- [34] S. J. Pauka, K. Das, R. Kalra, A. Moini, Y. Yang, M. Trainer, A. Bousquet, C. Cantaloube, N. Dick, G. C. Gardner, M. J. Manfra, and D. J. Reilly, A cryogenic CMOS chip for generating control signals for multiple qubits, *Nat. Electron.* **4**, 64 (2021).
- [35] X. Xue, *et al.*, CMOS-based cryogenic control of silicon quantum circuits, *Nature* **593**, 205 (2021).
- [36] Q.-M. Chen, Master's thesis, Tsinghua University, 2017.
- [37] D. G. Holmes and T. A. Lipo, *Pulse Width Modulation for Power Converters: Principles and Practice* (John Wiley & Sons, Hoboken, 2003), Vol. 18.
- [38] H.-J. Ding and R.-B. Wu, Robust quantum control against clock noises in multiqubit systems, *Phys. Rev. A* **100**, 022302 (2019).
- [39] This value is estimated by noting that $0.9999^{1000} \approx 0.9$.
- [40] L. Viola, E. Knill, and S. Lloyd, Dynamical decoupling of open quantum systems, *Phys. Rev. Lett.* **82**, 2417 (1999).
- [41] L. Viola, S. Lloyd, and E. Knill, Universal control of decoupled quantum systems, *Phys. Rev. Lett.* **83**, 4888 (1999).
- [42] S. Lloyd and L. Viola, Engineering quantum dynamics, *Phys. Rev. A* **65**, 010101 (2001).
- [43] H. F. Trotter, On the product of semi-groups of operators, *Proc. Am. Math. Soc.* **10**, 545 (1959).
- [44] M. Suzuki, Decomposition formulas of exponential operators and Lie exponentials with some applications to quantum mechanics and statistical physics, *J. Math. Phys.* **26**, 601 (1985).
- [45] A. D. Bandrauk and H. Shen, Improved exponential split operator method for solving the time-dependent Schrödinger equation, *Chem. Phys. Lett.* **176**, 428 (1991).
- [46] A. D. Bandrauk and H. Shen, Higher order exponential split operator method for solving time-dependent Schrödinger equations, *Can. J. Chem.* **70**, 555 (1992).
- [47] A. D. Bandrauk and H. Shen, Exponential split operator methods for solving coupled time-dependent Schrödinger equations, *J. Chem. Phys.* **99**, 1185 (1993).
- [48] R. McDermott and M. G. Vavilov, Accurate qubit control with single flux quantum pulses, *Phys. Rev. Appl.* **2**, 014007 (2014).
- [49] P. J. Liebermann and F. K. Wilhelm, Optimal qubit control using single-flux quantum pulses, *Phys. Rev. Appl.* **6**, 024022 (2016).
- [50] R. McDermott, M. G. Vavilov, B. L. T. Plourde, F. K. Wilhelm, P. J. Liebermann, O. A. Mukhanov, and T. A. Ohki, Quantum-classical interface based on single flux quantum digital logic, *Quantum Sci. Technol.* **3**, 024004 (2018).
- [51] E. Leonard, M. A. Beck, J. Nelson, B. Christensen, T. Thorbeck, C. Howington, A. Opremcak, I. Pechenezhskiy, K. Dodge, N. Dupuis, M. Hutchings, J. Ku, F. Schlenker, J. Suttle, C. Wilen, S. Zhu, M. Vavilov, B. Plourde, and R. McDermott, Digital coherent control of a superconducting qubit, *Phys. Rev. Appl.* **11**, 014009 (2019).
- [52] K. Li, R. McDermott, and M. G. Vavilov, Hardware-efficient qubit control with single-flux-quantum pulse sequences, *Phys. Rev. Appl.* **12**, 014044 (2019).
- [53] V. Jurdjevic and H. J. Sussmann, Control systems on Lie groups, *J. Differ. Equ.* **12**, 313 (1972).
- [54] A. J. Krener, A generalization of Chow's theorem and the bang-bang theorem to nonlinear control problems, *SIAM J. Control* **12**, 43 (1974).
- [55] H. J. Sussmann, A bang-bang theorem with bounds on the number of switchings, *SIAM J. Control Optim.* **17**, 629 (1979).
- [56] S. A. Vakhrameev, Bang-bang theorems and related questions, *Trudy Mat. Inst. Steklova* **220**, 49 (1998).
- [57] C. Moler and C. Van Loan, Nineteen dubious ways to compute the exponential of a matrix, twenty-five years later, *SIAM Rev.* **45**, 3 (2003).
- [58] J. A. Fleck, J. R. Morris, and M. D. Feit, Time-dependent propagation of high energy laser beams through the atmosphere, *Appl. Phys.* **10**, 129 (1976).
- [59] M. Feit, J. Fleck, and A. Steiger, Solution of the Schrödinger equation by a spectral method, *J. Comput. Phys.* **47**, 412 (1982).
- [60] M. D. Feit and J. A. Fleck, Solution of the Schrödinger equation by a spectral method II: Vibrational energy levels of triatomic molecules, *J. Chem. Phys.* **78**, 301 (1983).
- [61] See <https://www.keysight.com/fi/en/product/M8196A/92-gsa-s-arbitrary-waveform-generators.html> for data sheet.
- [62] K. K. Likharev and V. K. Semenov, RSFQ logic/memory family: A new Josephson-junction technology for subterahertz-clock-frequency digital systems, *IEEE Trans. Appl. Supercond.* **1**, 3 (1991).
- [63] X. Zhou, J. L. Habif, A. M. Herr, M. J. Feldman, and M. F. Bocko, A tipping pulse scheme for a rf-SQUID qubit, *IEEE Trans. Appl. Supercond.* **11**, 1018 (2001).
- [64] D. S. Crankshaw, J. L. Habif, T. P. Orlando, M. J. Feldman, and M. F. Bocko, An RSFQ variable duty cycle oscillator for driving a superconductive qubit, *IEEE Trans. Appl. Supercond.* **13**, 966 (2003).
- [65] V. K. Semenov and D. V. Averin, SFQ control circuits for Josephson junction qubits, *IEEE Trans. Appl. Supercond.* **13**, 960 (2003).

- [66] P. Zanardi and D. A. Lidar, Purity and state fidelity of quantum channels, *Phys. Rev. A* **70**, 012315 (2004).
- [67] L. H. Pedersen, N. M. Møller, and K. Mølmer, Fidelity of quantum operations, *Phys. Lett. A* **367**, 47 (2007).
- [68] X.-D. Yang, C. Arenz, I. Pelczer, Q.-M. Chen, R.-B. Wu, X. Peng, and H. Rabitz, Assessing three closed-loop learning algorithms by searching for high-quality quantum control pulses, *Phys. Rev. A* **102**, 062605 (2020).
- [69] We note that all the converted waveforms for AWG implementation can be further optimized to 0.9999 fidelity with conventional QOC algorithms.
- [70] N. Khaneja, R. Brockett, and S. J. Glaser, Time optimal control in spin systems, *Phys. Rev. A* **63**, 032308 (2001).
- [71] Q.-M. Chen, R.-B. Wu, T.-M. Zhang, and H. Rabitz, Near-time-optimal control for quantum systems, *Phys. Rev. A* **92**, 063415 (2015).
- [72] Q.-M. Chen, X. Yang, C. Arenz, R.-B. Wu, X. Peng, I. Pelczer, and H. Rabitz, Combining the synergistic control capabilities of modeling and experiments: Illustration of finding a minimum-time quantum objective, *Phys. Rev. A* **101**, 032313 (2020).
- [73] <https://github.com/chenqmion/QPWM>.